International Journal of Automotive Technology, Vol. 15, No. 5, pp. 823−833 (2014)
DOI 10.1007/s12239−014−0086−7

pISSN 1229−9138/ eISSN 1976−3832

MODEL FOR DYNAMIC BEHAVIOR OF THE CRANKSHAFT OF AN AIR COOLED DIESEL ENGINE SUBJECTED TO SEVERE FUNCTIONING

O. KEITA[1)*], T. HEDHLI[2)] and J. BESSROUR[2)]

[1)]Building Architecture and Town Planning Department (BATir), Université Libre de Bruxelles (ULB), Bruxelles 1050, Belgique
[2)]Laboratoire de Mécanique Appliquée et Ingenierie, Ecole Nationale d'Ingénieurs de Tunis, BP 37 Le Bélvédère, Tunis 1002, Tunisie

(Received 15 February 2013; Revised 8 May 2013; Accepted 30 September 2013)

ABSTRACT−The dynamic behavior of the engine organs in severe conditions is complicated to identify. In this paper, the dynamic behavior of the crankshaft of the diesel engine Deutz F8L413 direct injection-type air cooled in the severe operating conditions is investigated in a 3D global model. The maximum operating characteristics of the engine are experimentally measured on a bench test equipped with a hydraulic brake. The most stressed areas of the crankshaft are determined by numerical simulations. In addition, an analysis of the fatigue behavior of the crankshaft is carried out by using two fatigues criteria. The efficiency of the model is demonstrated by comparing between the numerical results and the experimental data obtained with the natural modes of vibration test.

KEY WORDS : Crankshaft, Dynamic behavior, Fatigue, Vibrations, Severe functioning

1. INTRODUCTION

The automotive crankshafts are subject to a large number of cyclic loading during their service, causing many fatigues and vibration problems. For the particular case of engines with cylinders in V-type, these dynamic phenomena are more important and merit to be clearly identified in the context of maximum engine load, i.e.to regimes corresponding to maximum power and torque.

Many researches were carried out in the field of dynamic crankshafts based on simplified models because of the complexity of the geometry and the many interactions involved. Large static and dynamic analyses were performed on the crankshaft to improve their durability (Henry *et al*., 1992) and performance (Dimbale *et al*., 2011). An algorithm is developed in (Nikolic *et al*., 2012) to obtain a theoretical wear diagram of IC engine crankshaft main bearings by considering the crankshaft as beam. A simulation of crankshaft dynamic behavior of engine with cylinders in V type was performed in (Niinoa *et al*., 2002) by measuring V-type experimentally using gauge the amplitude of stress at the crankpins for high and low engine speed. The research in (Çevik and Gürbüz, 2012) proved the effect of crankpin rolling on the fatigue behavior of ductile cast iron crankshaft used in diesel engines. Based on the staircase test methodology, they performed resonant bending fatigue tests to obtain stress versus number of cycles curves and to evaluate the fatigue endurance limits of ductile iron crankshaft under crankpin rolled and un-rolled conditions. One of the advantages of engines with cylinders in V-type configuration is that they greatly reduce the overall engine length, height and weight compared to an equivalent inline configuration. It was found that if the same 6 cylinder inline engine is converted into V-engine, the level of amplitudes of primary and secondary moments is reduced up to 50% (Ide *et al.,* 1990). A system model analyzing dynamic behavior of IC engine crankshaft has been developed in (Niinoa *et al*., 2002). The model couples the dynamic structure of the crankshaft, the hydrodynamics lubrication of the main bearings and the rigidity of the crankcase. Recently, an experimental study on engine dynamics Model based in-cylinder pressure estimation was carried out in (Feilong *et al*., 2012) and (Yu *et al*., 2013). A more complicated multi degree-of-freedom engine dynamic model was used in the works of (Taraza, 2002; Schagerberg and McKelcey, 2003; Larsson and Schagerberg, 2004) to estimate in-cylinder pressure by utilizing a crankshaft integrated torque sensor. However, only few researches has been conducted on 3D models of the crankshaft, especially on engines with cylinders in V-type under maximum loading conditions (regime of maximum power and torque). These real conditions of maximum loading allow realistic prediction of dynamic stress levels which is very important for durability, lightness and optimization of the dynamic responses (Kim and Woo, 2013). It is also important for resistance to

**Corresponding author.* e-mail: okeita@ulb.ac.be

fatigue as shown in (AR *et al*., 1989).

This paper investigates a 3D model using the maximum loading conditions deduced from experimental measurements on bench test to identify the dynamic behavior of a diesel engine crankshaft with cylinders in V-type taking as a case study Deutz diesel engine types F8L413 with four (4) crankpins to 90 widely spread. This engine, air-cooled, is heavily loaded. The novelty of the present model is that the parameters are derived from engine real working conditions which are used to identify the dynamic behavior of the crankshaft. This paper is organized as follows. First, identification of optimal regimes (maximum power and torque and minimum specific consumption) is made with experimental data collected on bench test. It is followed by the kinematic and dynamic characterization of the piston and the connecting rod this, is to determine the efforts exerted on the crankshaft through the connecting rod-crank handle system at maximum identified regimes. Then hydrodynamic bearing-crankshaft contact model is presented as well as the 3D finite element modeling of the crankshaft. The simulations results and post-processing are presented. The fatigue calculations are performed. The vibration modes were also identified. Vibration tests were conducted in laboratory to identify the eigen modes of free crankshaft (without flywheel) and compare to the eigen modes from numerical simulations.

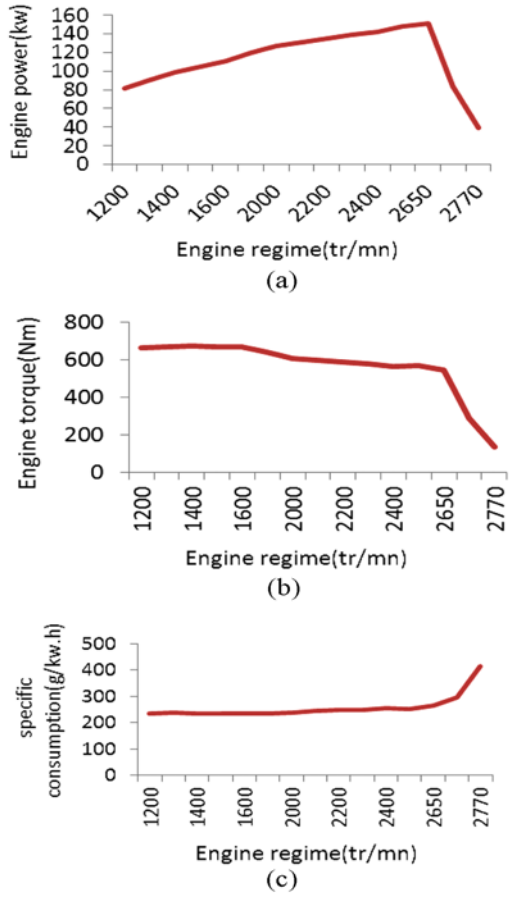

Figure 1. Engine regime: (a) power; (b) torque; (c) specific consumption.

2. EXPERIMENTAL STUDY ON BENCH TEST

The aim of bench test is to measure the operating parameters of the engine, in order to: (i)-plot external characteristics curves (power, torque, specific consumption) according to crankshaft number of turns; (ii) determine, through the connecting rod the acting efforts on the crankpins. The used fundamental material is a bench test equipped with a hydraulic brake. The test conditions and other materials prepared are described in (Taher, 2003). Figure 1 (a, b and c) show the curves of power, torque and specific consumption, respectively.

From these performance curves, it is find that 2650 tr/mm corresponds to the maximum power engine; 1600 tr/mm is minimum consumption and 1400 tr/mm is maximum torque. The crankshaft dynamic behavior is studied on those different regimes numerically by the finite element method.

3. KINEMATICS AND DYNAMICS CARACTERIZATION

3.1. Kinematic Characterization

The objective of this section is to determine the linear and angular accelerations of the connecting rod and the piston which is used in the crankshaft dynamic characterization. Figure 2 shows the technological diagram and parameterizations of the connecting rod-crank handle system.

The reference (**O**; **X; Y**; **Z**) is defined by the axis (**X; Y**) of the cylinder and the axis (**O**; **Z**) of the crankpin crank handle (Figure 2). It is assumed that the pulsation ω is practically constant (case of multi-cylinder engines). We denote by r the crank handle radius (OA), l is the length of connecting rod (AB) and $\lambda = r/l$=0.2632. Displacement of piston is y = OB. Projecting the contour of OAB on the axis (**O**; **X**), we obtain the relation between

θ and φ as follows:

$$\sin\varphi = -\lambda \sin \theta \qquad (1)$$

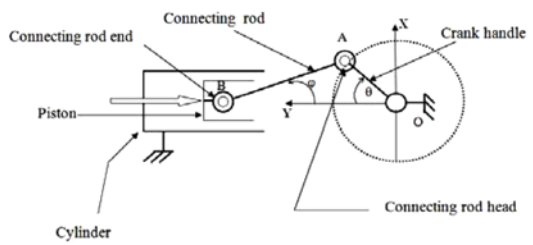

Figure 2. Technological scheme and parameterizations of connecting rod-crank handle system.

taking into account that $\cos\varphi \geq 0$(see Figure 2), we get:

$$cos\,\varphi = \sqrt{1-\lambda^2 \sin^2\theta} \tag{2}$$

3.1.1. Kinematics of the connecting rod

By deriving equation (1) and taking into account equation (2) we obtain angular acceleration of the connecting rod as

$$\ddot{\varphi} = \frac{\lambda\omega^2 \sin\theta}{(1-\lambda^2 \sin^2\theta)^{3/2}}(1-\lambda^2) \tag{3}$$

The linear acceleration of the connecting rod is therefore expressed by following relation:

$$\Gamma(G) = (\omega^2 r \sin\theta - l_G\ddot{\varphi}\cos\varphi + l_G\dot{\varphi}^2 \sin\varphi)\mathbf{x} - (\omega^2 r \cos\theta + l_G\ddot{\varphi}\sin\varphi + l_G\dot{\varphi}^2 \cos\varphi)\mathbf{y} \tag{4}$$

The detailed calculations of relations (3) and (4) are explained in Appendix A.

3.1.2. Kinematics of the piston

Projecting the contour of OAB on the (o, y) and taking into account equation (1), we obtain the acceleration of the piston as follows:

$$\ddot{y} = -\omega^2 r\left[\cos\theta - \frac{\lambda \sin^2\theta}{\sqrt{(1-\lambda^2 \sin^2\theta)}} + \lambda(1-\lambda^2 \sin^2\theta)^{3/2}\right] \tag{5}$$

3.2. Dynamic Characterization

Reduction elements of the mechanical actions applied to crankshaft crankpin and the piston are reduced on the axis of the crankpin and the connecting rod to a force and a momentum that is a function of the moving parts and their accelerations. To calculate this momentum, it is necessary to determine the mechanical actions applied to the connecting rod head and feet. The engine types F8L413 Deutz diesel is an engine with 8-cylinders in V-type. At each of the four crankpins are mounted to two head of connecting rod (figure 3). A multi-cylinder engine of V-type is constituted by two inline engines offset by an angle $\delta = (\mathbf{Y}_1,\mathbf{Y}_2)$ called the V opening angle (figure 3) (Swoboda *et al.*,1998). In our case V opening angle $\delta = 4\pi/8 = \pi/2$. Let $\mathbf{F}_{A1}$ and $\mathbf{F}_{A2}$ be the forces exerted by the crankpin on the connecting rods (b1) and (b2) at point A, respectively and $\mathbf{F}_{B1}$, and $\mathbf{F}_{B2}$ the forces exerted by the pistons on the connecting rods (b1) and (b2) at points B1 et B2 respectively.

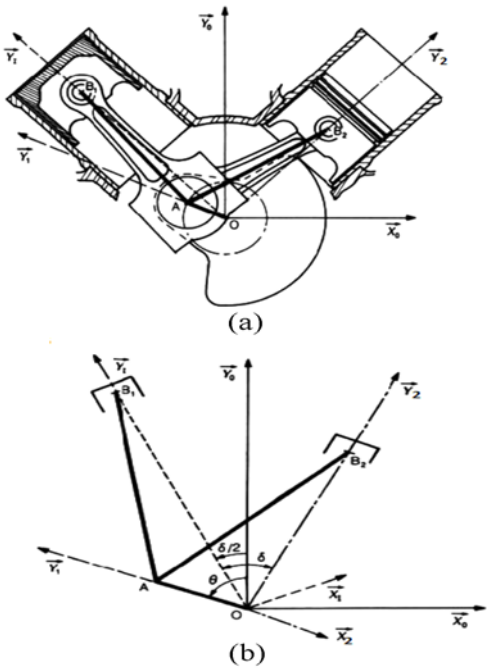

Figure 3. Defining reference for a engine with V- type cylinder: (a) Technological scheme; (b) Calculation scheme.

3.2.1. Case of the connecting rod (b1)

The reduction elements of the torsor quantities of accelerations of the connecting rod (b1) at its gravity center G1(which is also its inertia center) are $\delta_{G1}(b1)$ and $m_{b1}\Gamma(G_1)$ m_{b1}, is the mass of the connecting rod (b1), X_{A1} Y_{A1}, X_{B1} and Y_{B1} are projections of $\mathbf{F}_{A1}$ and $\mathbf{F}_{B1}$ respectively on $(\mathbf{O};\mathbf{X_1})$ and $(\mathbf{O};\mathbf{Y_1})$ axes (Figure 4). By applying the fundamental principle of dynamics to the connecting rod (b1), and projecting the equations on the different axes, we obtain the following equations:

$$m_{b1}.\Gamma(G1).\boldsymbol{X}_1 = m_{b1}.\ddot{x}_{G1} = X_{A1} + X_{B1} \tag{6}$$

$$m_{b1}.\Gamma(G1).\boldsymbol{Y}_1 = m_{b1}.\ddot{y}_{G1} = Y_{A1} + Y_{B1} \tag{7}$$

$$l_{G1}\cos\varphi_1.m_{b1}\ddot{x}_{G1} + l_{G1}\sin\varphi_1.m_{b1}.\ddot{y}_{G1} - lY_{B1}\sin\varphi_1 - l.X_{B1}\cos\varphi_1 = I_{G1Z1}\ddot{\varphi}_1 \tag{8}$$

3.2.2. Case of the piston of the connecting rod (b1)

By isolating the piston from the system, as in Figure 4, and applying the fundamental principle of dynamics we obtain:

$$\mathbf{F}_{B1} + \mathbf{P} + \mathbf{N} + \mathbf{F}_f = m_p.\Gamma\ (\boldsymbol{B}) \tag{9}$$

where $\mathbf{F}_{B1}$, is the action of connecting rod on the piston. **N**,

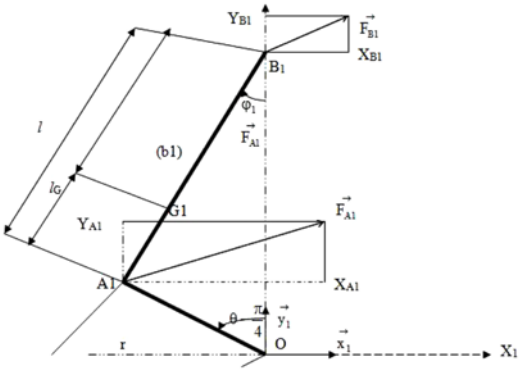

Figure 4. Calculation scheme for connecting rod (b1).

is the action of cylinder on the piston (reaction of the jacket). **P**, is the resulting combustion gas pressure uniformly distributed over the head of the piston and expressed as follows:

$$-\mathbf{P}\mathbf{Y}_1 = -\mathbf{P}(\theta).S.\mathbf{Y}_1 \tag{10}$$

in which $\mathbf{P}(\theta)$ represents differential pressure on both sides of piston. $\mathbf{F}_f$, is the frictional force between the jacket and the piston rings and is expressed as:

$$\mathbf{F}_f = -f\frac{\dot{\mathbf{Y}}_1}{|\ddot{\mathbf{Y}}_1|}|\mathbf{N}(\mathrm{M})| \tag{11}$$

Projecting equation (9) on the $(\mathbf{O};\mathbf{X}_1)$ gives the following equation:

$$N - X_{B1} \tag{12}$$

About the projection of equation (9) on the $(\mathbf{O};\mathbf{Y}_1)$ we obtain the following expressions depending upon whether the contact between the jacket and the piston occurs in push ($N \rightarrow |N| = N$) or opposite side ($N<0 \rightarrow |N| = N$):

$$-Y_{B1} - P \pm f\frac{\dot{\mathbf{Y}}_1}{|\dot{\mathbf{Y}}_1|}N = m_p.\ddot{y}_1 \tag{13}$$

The sets of equation (6,7,8,12,13,13) allow to determine the followings five liaison forces N, X_{B1}, Y_{B1} X_{A1} and Y_{A1} according to the gas pressure P, the coefficient of the friction between the piston and cylinder f, and the crankshaft rotation angle θ. Expressions of these forces are given in appendix A.

3.2.3. Case of the connecting (b2)

The calculation scheme to determine the forces exerted the crankpin on the connecting rod (b2) is identical to Figure 4 with different angles: $(\theta+\pi/4)$ instead of $(\theta+\pi/4)$. The expression of forces are similar to those obtained for the connecting rod (b1). Indeed $\ddot{\varphi}_1$ and $\dot{\varphi}_1$ are replaced by $\ddot{\varphi}_2$ and $\dot{\varphi}_2$. Their expression becomes respectively:

$$\ddot{\varphi}_2 = \frac{\lambda\omega^2\sin\left(\theta+\frac{\pi}{4}\right)}{\left[1-\lambda^2\sin^2\left(\theta+\frac{\pi}{4}\right)\right]^{3/2}}(1-\lambda^2) \tag{14}$$

and

$$\dot{\varphi}_2 = \frac{-\lambda\omega.\cos\left(\theta+\frac{\pi}{4}\right)}{\sqrt{1-\lambda^2\sin^2\left(\theta+\frac{\pi}{4}\right)}} \tag{15}$$

The forces on the piston of the connecting rod (b2) denoted $\mathbf{F}_{A2}$ of components X_{A2} and Y_{A2} are calculated taking into account equation (14 and 15). As the engine is an four crankpin engine, the forces on the other crankpins are calculated taking into account the phase difference between them. For the second, third and fourth crankpins, the expressions are the following:

$$\mathbf{F}_A\left(\theta+\frac{\pi}{2}\right),\ \mathbf{F}_A\left(\theta+2\frac{\pi}{2}\right),\ \mathbf{F}_A\left(\theta+3\frac{\pi}{2}\right) \tag{16}$$

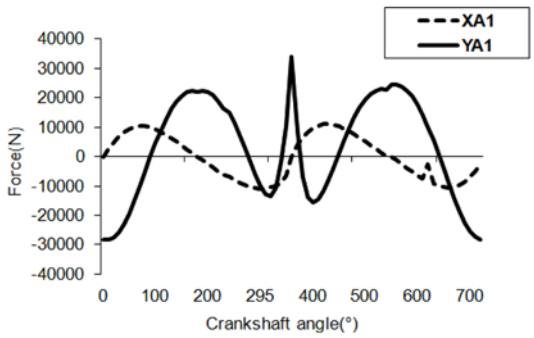

Figure 5. Force exerted by connecting rod (b1) on the crankpin 1.

Figure 5 represents the evolution of the force exerted by the connecting rod (b1) on crankpin 1 according to crankshaft rotation angle θ.

During the admission and compression process (between 0 and 360°) and evacuation (between 540° and 720°) the component of the force exerted by the connecting rod (b1) on the crankpin 1 (Y_{A1}) varies sinusoid ally. While in the process of combustion and expansion (between 360° and 540°) it varies non-harmonic. Regarding to the component (X_{A1}), the appearance is nearly sinusoidal.

3.2.4. Study of engine torque

By definition, the engine torque is the product of force applied perpendicular to the crankpin by the connecting rod on the crankpin by the radius $R = Piston\ stricke/2$. Considering the connecting rod (b1) in reference related to the axis of its cylinder and associating to a reference to the crankpin (Figure 6), we calculate the torque created by the connecting rod (b1) on the crankpin1as following (Figure 6):

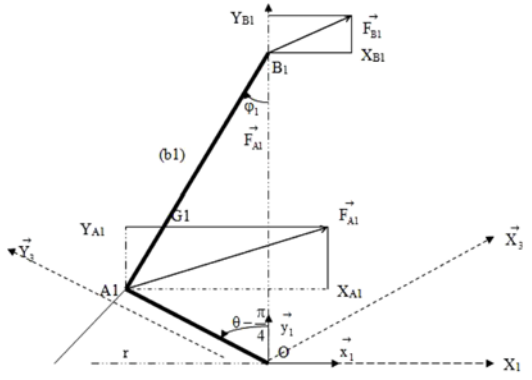

Figure 6. Calculation scheme the engine torque created by connecting rod (b1).

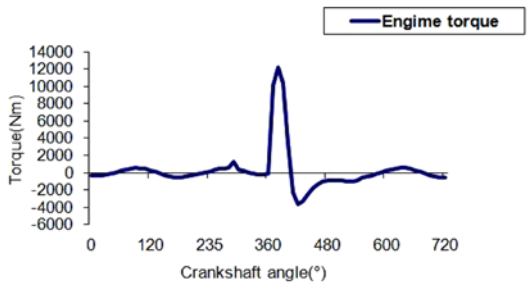

Figure 7. Engine torque created by the first.

$$T_{engine} = R\left(X_{A1}\cos\left(\theta-\frac{\pi}{4}\right)+Y_{A1}\sin\left(\theta-\frac{\pi}{4}\right)\right) \quad (17)$$

By analogy the engine torque created by connecting rod (b2) on crankpin 1 is:

$$T_{engine} = R\left(X_{A2}\cos\left(\theta+\frac{\pi}{4}\right)+Y_{A2}\sin\left(\theta+\frac{\pi}{4}\right)\right) \quad (18)$$

Finally, the total engine torque on the crankpin 1 is at each instant equal to the sum of the torques generated by the two connecting rods. The torque on other crankpins is determined in the identical way, by taking into account the phase difference between two crankpins (equation (16)). Figure 7 shows that during the admission and the compression process (between 0° and 360°), the engine torque produced by the first cylinder is relatively low. While the expansion process corresponds to higher values of the torque. This could be due to the high pressure gas combustion in the cylinders that causes significant efforts on crankpins. During the evacuation process, the torque becomes low. The variation of the engine torque as a function of the crankshaft rotation angle on the different crankpins and variation of the resulting engine torque (superposition on each crankpin torque) are shown in Figure 8 (a and b).

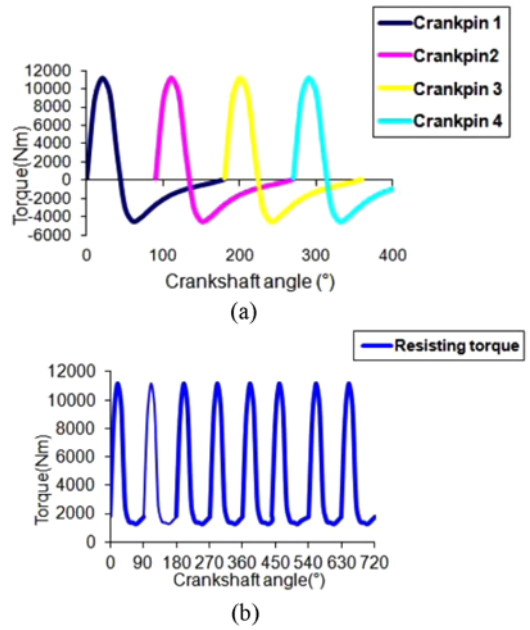

Figure 8. Variation with the crankshaft angle: (a) of the engine torque on the various crankpins; (b) of the total engine torque resulting from the superposition of the torques created on the four crankpins.

4. MODELING OF BEARING –CRANKSHAFT

In this section, we determine the reactions of bearing on the crankshaft. In our case, the hydrodynamic bearing model is used. A smooth bearing consists of a shaft which rotates within a bearing bush separated to the latter by a film of fluid. Under the action of a load, the center of the bearing bush and the shaft do not coincide, and there is a convergent-divergent corner in the film. The rotation of the shaft drives the fluid in the converging wedge and creates a pressure field that opposes to the load and balances it. This model focuses on the hydrodynamic regime and assumes that the fluid flow through the bearing is isothermal and laminar. Figure 9 shows the schemes for calculating the hydrodynamic pressure force of oil film. According to the assumptions shown in Figure 9 and for the incompressible

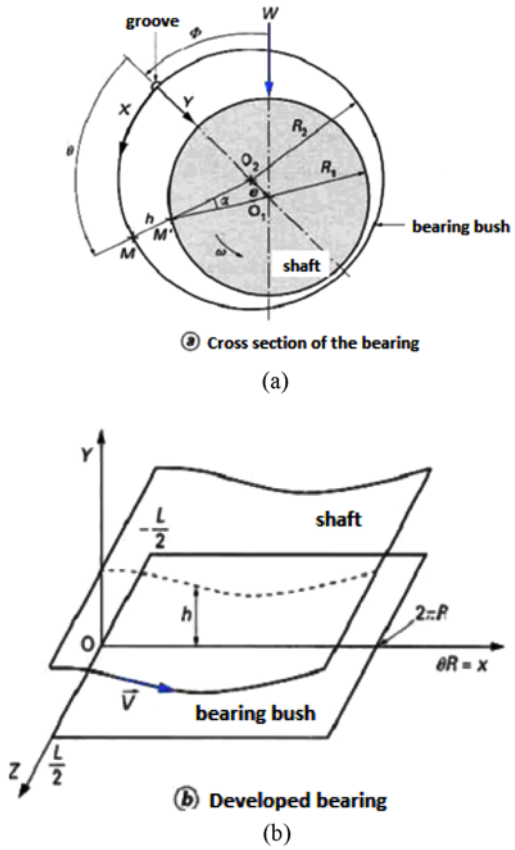

Figure 9. Scheme and assumptions of computation of the hydrodynamic pressure of the oil film exerted on the crankshaft: (a) hydrodynamic bearing; (b) bearing bush assimilate to a plan (Jean, 1995).

and iso-viscosious fluid permanent regime, Reynolds equation is given (Jean, 1995) as:

$$\frac{1}{R^2}\frac{\partial}{\partial\theta}\left(h^3\frac{\partial P}{\partial\theta}\right)+\frac{\partial}{\partial z}\left(h^3\frac{\partial P}{\partial z}\right)=\frac{6\mu V}{R}\frac{dh}{d\theta} \quad (19)$$

Where P, is the pressure in the lubricant, θ and Z, are the circumferential and axial coordinates, respectively, and expressed as $\theta = X/R$ h, is the lubricant film thickness $V = \omega R$, is the linear velocity of the shaft μ, is the dynamic viscosity of fluid. ε, is the relative eccentricity ($\varepsilon = e/C$), which varies between 0 and 1. The film thickness can be written as:

$$h = C(1+\varepsilon\cos\theta) \quad (20)$$

Where C, is radial gap and expressed as: $C=R_2 - R_1$.

Considered the boundary conditions of Stierber and Swift that are, also referred to Reynolds conditions, in the case of infinitely short bearing, and taking into account the boundary condition of Gambel that assumes the pressure zone is limited to the convergent part of the film (Jean, 1995). The pressure field can be expressed as follows:

$$P(\theta) = \frac{3\mu V}{C^2 R}\left(\frac{L^2}{4}\right)\frac{\varepsilon\sin\theta}{(1+\varepsilon\cos\theta)^3} \quad (21)$$

where L, is the length of the bearing (Figure 9). $C = 0$; 1mm. The value of ε is obtained from the abacuses according to the ratio L / D of length to the diameter of bearing and the dimensionless value of the constant load acting on the bearing (Jean, 1995) S, defined as the following equation:

$$S = \frac{\mu L D}{W}\left(\frac{R}{C}\right)^2 \quad (22)$$

where W, is the constant load on the bearing. In our case, S is the weight of the crankshaft supported by a bearing.

5. MODELING AND SIMULATION OF THE CRANKSHAFT DYNAMIC BEHAVIOR

In this section, we present a numerical investigation of the dynamic behavior of the crankshaft by the finite element method with numerical code ABAQUS.

5.1. Mesh

The geometric model has been developed on CAO software and imported into the finite element analysis code. The mesh is adopted in linear by using tetrahedral element types (C3D4) and, contains 36.215 nodes and 149.062 elements.

5.2. Crankshaft Loading Modelization

(i)-The efforts on the crankpins which the correct application is an important point. These efforts are modeled by some efforts representative at nodes for which it is necessary to make certain distribution assumptions. In fact, the charged surfaces are interchanged in two consecutive time-cycle engines. The surface distribution of efforts has been used. On the crankpins, the loads are the reaction forces of the crankpins against the connecting rods calculated from the dynamic characterization as proposed in section 3. (ii) -The inertia forces of rotation applied in the entire volume of the crankshaft. (iii)- The resistive torque on the flywheel. (iv) -The hydrodynamic pressure forces of oil film resulting from bearing -crankshaft boundary conditions. Figure 10 represents the mesh and applied loads on the crankshaft. For the dynamic calculation, we use the dynamics implicit scheme. The mechanical properties of the crankshaft are summarized in Table 1.

Table 1. Crankshaft mechanical properties.

Material	E (N/mm²)	ν[-]	ρ (k/m³)	Yield (Mpa)
42CD4	200.000	0.3	7800	780

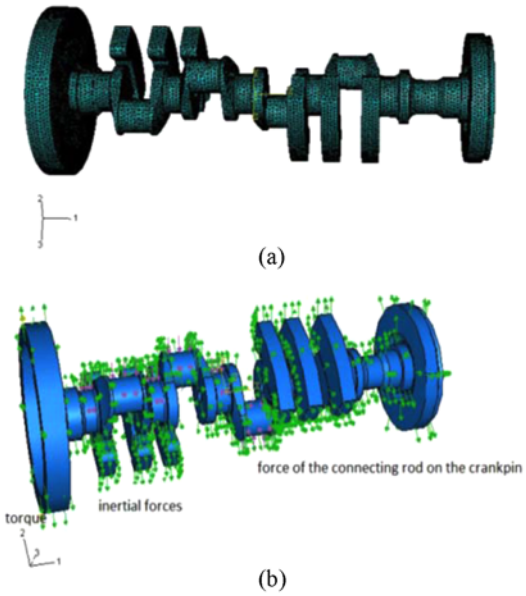

Figure 10. Crankshaft modeling: (a) Mesh; (b) mechanical load applied on crankshaft.

5.3. Numerical Results

Among the numerical results from the simulations, we extract essentially the von Mises equivalent stress. These results allow us to analyze the fatigue under cyclic loading (by using the von Mises equivalent stress). Figure 11 shows the state of the von Mises equivalent stress for some instants of the cycle. It proves that high stress zones are at the crankpin 3. This may be due to the fact that the crankpin 3 occupies the central position of the crankshaft, more solicited by bending stresses. The fatigue analysis of the crankshaft is performed at this crankpin. The Figure 12 shows the evolution over time of the most severely stressed

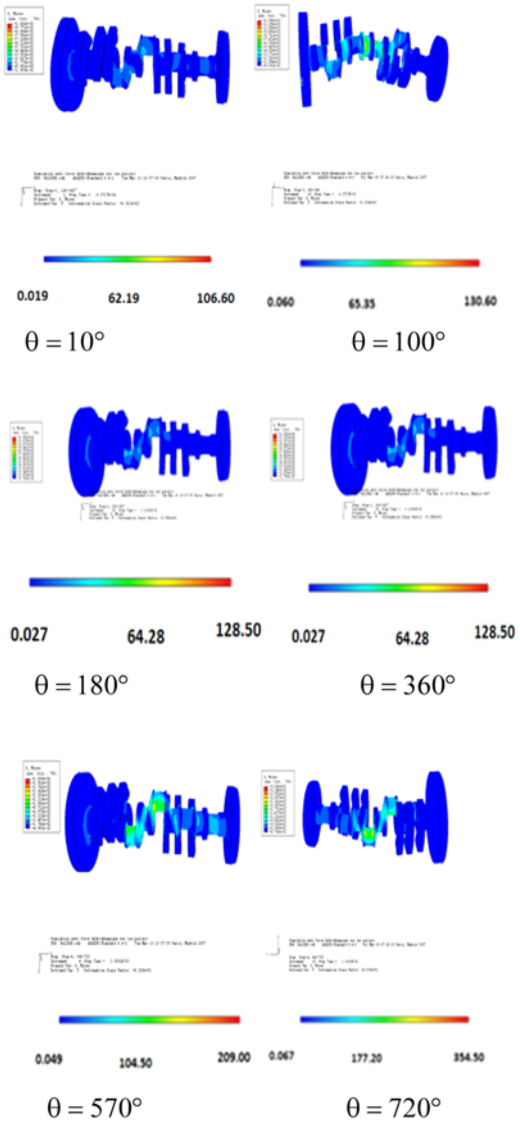

Figure 11. Von Mises stress for some times of the cycle.

point of the crankpin 3. We can observe fluctuations, as it is the case of any part submitted to various stresses over time. In practice for the calculation, these fluctuations are sinusoidally modelized. The maximum value of the stress in this point is 46 MPa (Figure 12), which remains significantly lower than the yield stress of the crankshaft material: R_e = 870 MPa.

5.4. Verification in Fatigue

As indicated in Section 1, the aim of this section is to identify the fatigue behavior of the crankshaft under maximum engine loading conditions (N = 2650 tr/mn). The crankshaft during its motion is subjected to dynamic and cyclic loads. These solicitations induce cyclical stresses. It follows that the breakage of the part occurs after a number of cycles N for a stress amplitude below the static tensile

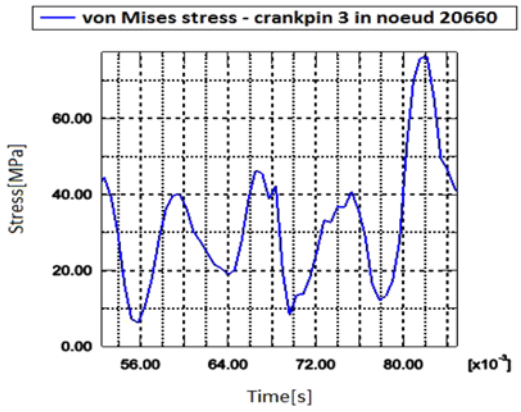

Figure 12. Evolution over time of σ_{Mises} at the most stressed point of crankpin.

strength of the material: this is the fatigue phenomenon. This situation leads to premature appearance of damage (cracking or fracture).

The fatigue analysis are a group of stresses and strains post treatment analyses oriented towards to an appreciation of the safety factor, which reflects the durability or endurance. For the fatigue analysis, we use the following fatigue criterion: Haigh and Dang Van criterion.

5.4.1. Fatigue verification with Haigh criterion

Endurance diagram of abscissa, mean stress denoted σ_a and ordinate alternating stress denoted σ_m are from the Wöhler curves (Figures 13). It defines the set of endurance limits σ_D depending on the value of the average stress for a given number of cycles (Jean, 1995). For the fatigue analysis and to define a safety factor of mechanical parts on can use the Haigh diagram. This diagram represents the amplitude of alternating stress depending on the mean stress. The construction of diagram can be performed in two ways, either from the Goodman line (used in our model) or from the Gerber parable. In both cases, the factor of safety with respect to the fatigue limit or endurance is determined using the following equations (Figure 13):

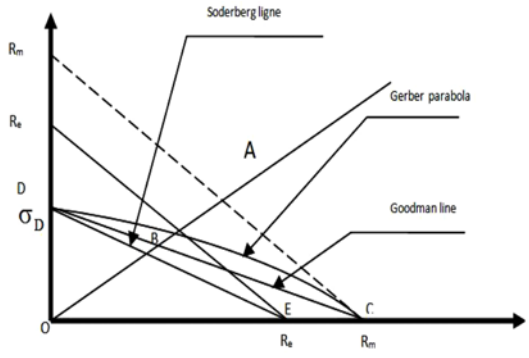

Figure 13. Endurance diagram (Gazaud *et al*., 1969).

$$(C, D) : y = \frac{\sigma_D}{R_m}x + \sigma_D \quad (23)$$

$$(D, E) : y = -x + R_e \quad (24)$$

$$(D, A) : y = \frac{\sigma_a}{\sigma_m}x \quad (25)$$

Point B is the intersection of the line (O, A) with line of the Goodman (C, D). Point A can occupy different positions on the line (O, A). The safety coefficient is defined as:

$$S = \frac{OB}{OA} \quad (26)$$

The choice of the stress fatigue limit σ_D, breaking strength σ_m and yield strength R_e is made according to the steel grade of the crankshaft, number of cycles, and its diameter (Jean-Pierre, 2008). For our crankshaft of 42CD4 grade, corresponding value are: $\sigma_D = 600$ MPa, for 10^7cycles; $\sigma_m = 1200$ MPa, and $R_e = 870$ MPa. The determination of the equation of the line (O,A) requires knowledge of mean and alternating stress (equation (25)). For that we use the evolution curve of von Mises equivalent stress (Figure 12). The development at first order in Fourier series of von Mises stress is expressed as:

$$\sigma_{eq}(x, y, z, t) = ((\sigma_{eq}) + (\sigma_{eq})_a \sin(\omega t + \varphi)) \quad (27)$$

where,

$$(\sigma_{eq})_m = \int_0^T \sigma_{eq}(x, y, z, t)dt \quad (28)$$

and

$$(\sigma_{eq})_a = \frac{2}{T}\left(\left(\int_0^T \sigma_{eq}(x, y, z, y)\cos\omega t dt\right)^2 + \left(\int_0^T \sigma_{eq}(x, y, z, y)\sin\omega t dt\right)^2\right)^{1/2} \quad (29)$$

are the mean and alternating stress, respectively. We use the graphical method of trapezoids to compute integrals in equation (28 and 29). For the maximum power of regime, the cycles number is: 1cycle = 4π = 12.56rd. For N regime, it corresponds to n cycles /s. n=N/2*60 = 22.08 cycles/s for maximum power regime, where the pulsation ω = 138.66rd. Our factor of safety research is focus on a number of points where the equivalent stress is maximum at a given time in the cycle. Figure 14 shows the fatigue verification with Haigh criterion at the crankpin 2 and 3.

5.4.2. Fatigue verification with Dang Van criterion

The Dang Van criterion is one of the multi-axial fatigue criteria. A multiaxial fatigue criterion indicates whether the endurance limit or more generally the fatigue limit of the material in N cycles is reached for a succession of stress states defining a multi-axial cycle. This criterion is a global

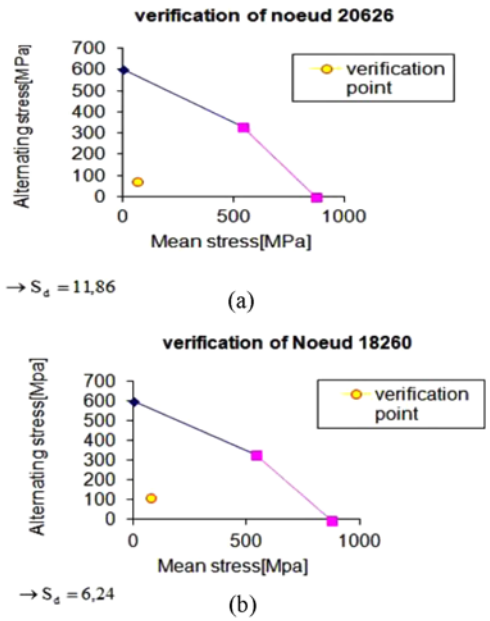

Figure 14. Haigh diagram: (a) at crankpin 2, (b) at crankpin 3.

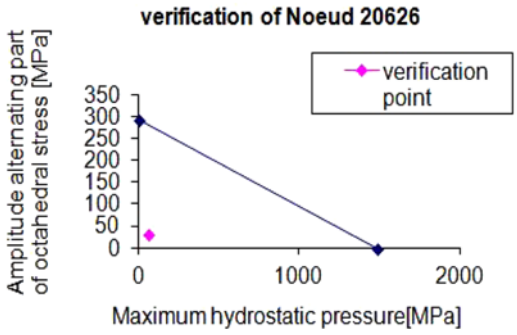

Figure 15. Fatigue verification at the crankpin 2. Dang van Diagram.

approach. It proposes a linear relationship between the amplitude $\tau_a(t)$ (alternating part) of octahedral shear stress and hydrostatic pressure $p_H(t)$, and is expressed as follows (Bouraoui *et al.*, 2007):

$$\max_n(\max_t)\{[\tau_a(t)] + \alpha_D p_H(t)\}) \le \beta_L \quad (30)$$

$\tau_a(t)$ is define by the following equation:

$$\tau_a(t) = \tau_a(t) - \tau_m \quad (31)$$

where $\tau(t)$ and τ_m are macroscopic and average split, respectively. $\tau(t)$ can be expressed as:

$$\tau(t) = \frac{1}{3}\sqrt{(\sigma_1 - \sigma_2)^2 + (\sigma_2 - \sigma_3)^2 + (\sigma_3 - \sigma_1)^2} \quad (32)$$

The constants α_D and β_D are determined from reference

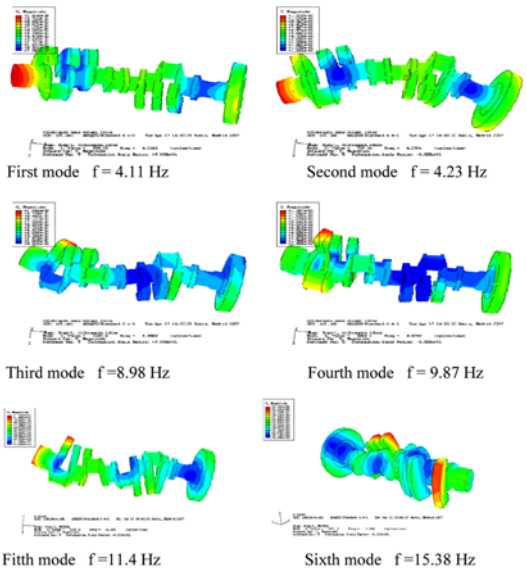

Figure 16. Representation of free crankshaft eigen modes without engine flywheel for the first sixth modes.

fatigue tests (Gazaud *et al*., 1969). (see details in Appendix A). The fatigue resistance condition is defined as:

$$\tau_a + 0,198\ p_{H\max} \leq 294,3 \qquad (33)$$

The Figure 15 illustrates Dang van diagrams at thecrankpin 2

6. MODAL ANALYSIS OF THE CRANKSHAFT

6.1. Numerical Study

Vibration analysis of the first six modes of the free crankshaft (without flywheel) is shown in Figure 16. The first vibration mode (f = 4.11 Hz) corresponds to bending in the vertical plane with two nodes of vibration which are relatively symmetrical to the crankshaft center. The second vibration mode (f = 4.23 Hz) is a bending mode in the horizontal plane also with two vibration nodes relatively symmetrical to the crankshaft center. The fourth vibration mode (f = 9.87 Hz) is a torsional mode along the axis of the crankshaft with a single node near by the engine flywheel: is the first torsional mode. The fifth vibration mode (f = 11.49 Hz) is a bending mode in the vertical plane with three vibration nodes.

6.2. Experimental Study

The test is performed in the laboratory of mechanical vibration of Ecole Nationale d'ingénieurs de Tunis (ENIT). The aim of this test is to compare the free crankshaft frequencies with the numerical simulation results. We used the impulse shock close to a Dirac due to its ease of production and rapidity. We use the averaging technique of a predetermined number of spectra to eliminate the noise.

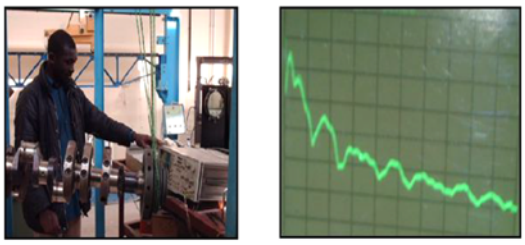

Figure 17. (a) Experimental device and test underway, (b) frequency spectrum of the Fourier transform of the response to the excitation.

The measurements only last a few seconds. The mathematical representation of an ideal shock is realized by the infinitely short DIRAC function of which amplitude spectrum is constant over the entire frequency range. The experimental device consists of a piezoelectric sensor (accelerometer) which captures vibration signal on the crankshaft excited in impulsive mode. The signal from the sensor is transformed by a signal conditioner which comprises: (i) a measuring transducer which converts signal into electric current easily transportable, serves as an input and is powered by a 12 volt source. (ii) an amplifier is designed to increase the signal intensity and to make it less sensitive to the noise of ambient background. It serves as an output signal, and it is connected to the Fourier transformer. A source of current supply of 12 volts is connected to the converter. A spectrum analyser, fast Fourier transform, gives the Fourier transform of temporal signal. Figure 17 (a) shows the experimental device used for the completion of vibration test, and Figure 17. b demonstrates the frequency spectrum of the Fourier transform response.

6.2.1. Measurement results

After repeated the test several times on a frequency band of 50 Hz, the first eigen frequencies obtained with the free crankshaft without engine fywheel are: 4.6 Hz; 8.7 Hz; 11.8 Hz; 17.8 Hz. and 21.4 Hz. Table 2 shows the comparison between the first five eigen frequencies determined in the test and the values computed by numerical simulations.

6.3. Interpretation of Test Results

The relative error between the eigen frequencies for experimental and numerical values, varies from five (8 –

Table 2. Comparison of experimental and numerical eigen frequencies.

	M1 (HZ)	M2 (HZ)	M3 (HZ)	M4 (HZ)	M5 (HZ)
Experimental frequencies	4.6	8.6	11.8	17.8	21.4
Mumerical frequencies	4.11	8.9	9.87	18.1	23.07

16.35) %. These errors could be due the one hand, to the fact that the geometric model is an idealized geometry of the crankshaft, not taking into account all its real form, and secondly, they may come from: (i) systematic error; a typical example is the drift time of the sensor sensitivity. (ii) the parasite error; it is defined in standard NF X 07-001 as a gross error resulting from improper execution of measurement. Table 2. Comparison of experimental and numerical eigen frequencies.

7. CONCLUSION

This paper has enabled the development a numerical model of three dimensional global dynamic behavior of the crankshaft by finite elements of a diesel engine air cooled. To achieve this goal, we carried out a kinematic and dynamic analysis to determine the forces and moments on different crankpin of the crankshaft. Description of the stress fields of mechanical origin, led to the identification of t most solicited zones which are the risk zones. To validate the dynamic endurance, a analysis of the fatigue behavior was carried out in these zones. That, using Haigh criterion and also the multiaxial fatigue criterion of Dang Van that takes into account the multiaxial cyclic loading of crankshaft. Simulation of vibration behavior by finite elements of free crankshaft allowed identifying eigen modes and frequencies. An experimental vibration test conducted on free crankshaft able to validate the model by comparing the eigen frequencies experimentally obtained to those found in numerical simulation. Comparison of values is relatively good.

ACKNOWLEDGEMENT–We thank Islamic developpement Bank (IDB) scholarship program for financially support this work.

REFERENCES

Bouraoui, C., Fathallah, R., Khantouch, Z., Châteauneuf, A. and Destrebeq, J. F. (2007). Analyse comparative des critères de fatigue multiaxiale basée sur une approche fiabiliste: Etude de cas. *Congrès CMSM 2007*. Monastir, Tunisie.

Çevik, G. and Gürbüz, R. (2012). Evaluation of fatigue performance of a fillet rolled diesel engine crankshaft. *Engineering Faliure Analysis*, **27**, 250–061. http://dx.doi.org/10. 1016/j.engfailanal.2012.07.026

Dimbale, N., Bhujbal, A., Hanabar, R., Gawande, S. H., Navale, L. G. and Daphal, G. (2011). Dynamic vibration analysis for multi-cylinder diesel engine of SL90 type. *Int. J. Science and Advanced Technology* **1**, **2**, 55–61.

Feilong, L., Gehan, A. J., Nick, C. and Ahmed, S. (2012). An experimental study on engine dynamics model based in-cylinder pressure estimation. *SAE Paper No*. 2012-01-0896.

Gazaud, R., Pomey, G., Rabbe, P. and Janssen, C. H. (1969). *La Fatigue des Metéaux*. DUNOD. Paris.

Heath, A. R. and McNamara, P. M. (2008). Crankshaft stress analysis - The combination of finites element and classical techniques. *J. Eng. Gas Turbines Power* **112**, **3**, 268–275.

Henry, J. P., Toplosky, J. and Abramczuk, M. (1992). Crankshaft durability prediction a-new 3D approach. *SAE Paper No*. 920087.

Ide, S., Uchida, T., Ozawa, K. and Izawa, K. (1990). Improvement of engine sound quality through a new flywheel system exibly mounted to the crankshaft. *SAE Paper No.* 900391.

Jean, F. (1995). Butées et Paliers hydrodynamique. Techniques de L'ingénieur. B-5320.

Jean-Pierre, P. (2008). Moteur Diesel D'automobiles, Conception et Mise en Point. Techniques de L'ingérieur. BM-2575.

Jian, L. and Henri-Paul, L. (1998). Concentration de Contraintes. Techniques de L'ingénieur. BM-5040.

Kim, M. S. and Woo, Y. H. (2013). Robust design optimization of the dynamic responses of a tracked vehicle system. *Int. J. Automotive Technology* **14**, **1**, 47–51.

Larsson, S. and Schagerberg, S. (2004). SI-engine cylinder pressure estimation using torque sensors. *SAE Paper No*. 2004-01-1369.

Nikolic, N., Torovic, T. and Antonic, Z. (2012). A procedure for constructing a theoretical wear diagram of IC engine crankshaft main bearings. *Mechanism and Machine* Theory, **58**, 120–136.

Niinoa, T., Iwamoto, T. and Ueda, S. (2002). Development of simulation technology for dynamic behavior of crankshaft systems in motorcycle engines. *JSAE Review*, **23**, 127–131.

Schagerberg, S. and McKelvey, T. (2003). Instantaneous crankshaft torque measurements - Modeling and validation. *SAE Paper No.* 2009-01-0713.

Swoboda, B. (1998). *Mécanique des Moteurs Alternatifs*. Institut Française du Pétrole. Edn. Technip. Paris.

Taher, H. (2003). Un Modèle Thermomécanique d'un Moteur à Combustion Interne Refroidi Par Air. Mémoire de DEA. ENIT.

Taraza, D. (2002). Accuracy limits of IMEP determination from crankshaft speed measurements. *SAE Paper No*. 2002-01-0331.

Yu, S., Choi, H., Cho, S., Han, K. and Min, K. (2013). Development of engine control using the in-cylinder pressure signal in a high speed direct diesel engine. *Int. J. Automotive Technology* **14**, **2**, 175–182.

APPENDIX

A. Kinematics of the Piston and the Connecting Rod

Appendix A.1. Kinematics of the connecting rod

The velocity field of a solid being a equiprojectif vector field, we can write:

$$\boldsymbol{v}(\mathrm{G}) = \boldsymbol{v}(A) + \Omega \wedge \boldsymbol{AG} \tag{A1}$$

Where,

$$\Omega = \dot{\varphi} \cdot \boldsymbol{z} \tag{A2}$$

is, rotation vector of the connecting rod $\boldsymbol{v}$(G) is, velocity of the gravity center G and $\boldsymbol{v}$(A) is, Velocity of point A. However, the velocity of point A linked to the connecting rod is equal to the velocity of point A linked to the crankpin (A being the geometrical point of connecting rod-crankpin contact, see diagram), whence:

$$\boldsymbol{v}(A) = -(\omega r \cos\theta) \cdot \boldsymbol{x} - (\omega r \sin\theta) \cdot \boldsymbol{y} \tag{A3}$$

knowing that:

$$AG = l_G \sin\varphi \boldsymbol{x} + l_G \cos\varphi . \boldsymbol{y} \tag{A4}$$

Equation (A.1) lead to:

$$v_G = -(\omega r . \cos\theta + \dot{\varphi} l_G \cos\varphi) . \mathbf{x} - (\omega r \sin\theta + \dot{\varphi} l_G \sin\varphi) . \boldsymbol{y} \tag{A5}$$

By deriving equation (A.5) with respect to time and remembering that ω is considered constant, we obtain equation (5) as mentioned in section 3

Appendix A.2. Kinematic of the Piston

Projecting the contour of OAB on the axis (**O**; **y**) and taking into account equation (1), we obtained elongation of the piston as follows:

$$y = r\cos\theta + l\sqrt{(1 - \lambda^2 \sin^2\theta)} \tag{A6}$$

By deriving equation (A.6) with respect to time one obtains the velocity of the piston as follows:

$$y = -\omega r \sin\theta \left[1 + \frac{\cos\theta}{\sqrt{(1 - \lambda^2 \sin^2\theta)}}\right] \tag{A7}$$

Deriving a second time equation (A.6) and taking account equation (1), we obtain the acceleration of the piston

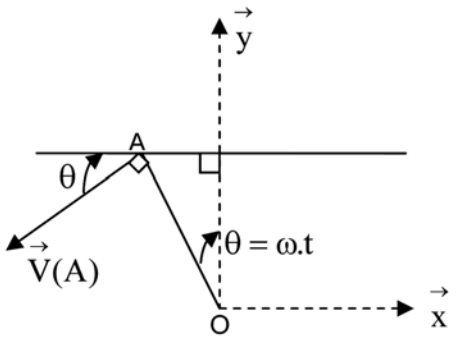

Figure A18. velocity scheme.

(equation (6)) as defined in section 3

Appendix A.3. Determination of the Unknown Liaison Forces

By solving the sets of equations (6,7,8,12,13,13) in section 3 we obtain:

$$X_{B1} = N \tag{A8}$$

For the case of N > 0 ($\theta \in [0, 2\pi] \cup [2\pi, 3\pi]$)

Y_{B1} is obtain in the following expression:

$$Y_{B1} = -m_p . \ddot{y}_1 - P - f \frac{\dot{y}_1}{|\dot{y}_1|} N \tag{A9}$$

Substitution of equation (A.9) into equation (9) (in section 3) lead to the following expression:

$$N = \frac{I_{G1Z1} \ddot{\varphi}_1 - l_{G1} . m_{b1} (\cos\varphi_1 . \ddot{x}_{G1} + \sin\varphi . y_{G1}) + l \sin\varphi_1 . (-m_p . \ddot{y}_1 + P)}{(f \frac{\dot{y}_1}{|\dot{y}_1|} . \sin\varphi_1 . l - l\cos\varphi)} \tag{A10}$$

For the case of N<0 ($\theta \in [0 - \pi, 2\pi] \cup [3\pi, 4\pi]$) similarly we find Y_{B1} as:

$$Y_{B1} = -m_p \cdot \ddot{y}_1 - P - f \frac{\dot{y}_1}{|\dot{y}_1|} N \tag{A11}$$

In this second case N is expressed as:

$$N = \frac{I_{G1Z1} \ddot{\varphi}_1 - l_{G1} . m_{b1} (\cos\varphi_1 . \ddot{x}_{G1} + \sin\varphi . y_{G1}) + l \sin\varphi_1 . (-m_p . \ddot{y}_1 + P)}{(-f \frac{\dot{y}_1}{|\dot{y}_1|} . \sin\varphi_1 . l - l\cos\varphi)} \tag{A12}$$

The components of the force exerted by the crankpin on the connecting rod (b1) X_{A1} and Y_{A1} can then be determine by following below expressions:

$$X_{A1} = m_{b1} \ddot{x}_{G1} - X_{B1} \tag{A13}$$

$$Y_{A1} m_{b1} \ddot{y}_{G1} - Y_{B1} \tag{A14}$$

Appendix A.4. Determination of the Constants α_D and β_D for Dan Van Fatigue Criterion

Constants α_D and β_D are determined from reference fatigue tests and expressed as:

$$\alpha_D = \frac{t_{-1} - f_{-1}/2}{f_{-1}/3} \tag{A15}$$

$$\beta_D = t_{-1} \tag{A16}$$

t_{-1} and f_{-1} are the endurance limits in torsion and alternating bending, respectively. For the material of the crankshaft 42CD4 : t_{-1} = 294.3 MPa, f_{-1} = 519.93 MPa. This allows to find α_D =0.198 and β_D =294.3.